10756 *Biochemistry* **2010,** *49,* 10756–10764
DOI: 10.1021/bi101318m

BIOCHEMISTRY
including biophysical chemistry & molecular biology
Article

Molecular Level Interaction of the Human Acidic Fibroblast Growth Factor with the Antiangiogenic Agent, Inositol Hexaphosphate[†,‡]

Sriramoju M. Kumar,[§] Han-Min Wang,[§] Sepuru K. Mohan,[§] Ruey-Hwang Chou,[∥,⊥] and Chin Yu*[,§]

[§]*Department of Chemistry, National Tsing Hua University, Hsinchu, Taiwan,* [∥]*Center for Molecular Medicine, China Medical University Hospital, Taichung 404, Taiwan, and* [⊥]*Department of Biotechnology, Asia University, Taichung 413, Taiwan*

Received August 17, 2010; Revised Manuscript Received November 11, 2010

ABSTRACT: Acidic fibroblast growth factor (FGF1) regulates a wide array of important biological phenomena such as angiogenesis, cell differentiation, tumor growth, and neurogenesis. Generally, FGFs are known for their strong affinity for the glycosaminoglycan heparin, as a prerequisite for recognition of a specific tyrosine kinase on the cell surface and are responsible for the cell signal transduction cascade. Inositol hexaphosphate (IP6) is a natural antioxidant and is known for its antiangiogenic role, in addition to its ability to control tumor growth. In the present study, we investigated the interaction of IP6 with the acidic fibroblast growth factor (FGF1) using various biophysical techniques including isothermal calorimetry, circular dichroism, and multidimensional NMR spectroscopy. Herein, we have reported the three-dimensional solution structure of the FGF1−IP6 complex. These data show that IP6 binds FGF1 and enhances its thermal stability. In addition, we also demonstrate that IP6 acts as an antagonist to acidic fibroblast growth factor by inhibiting its receptor binding and subsequently decreasing the mitogenic activity. The inhibition likely results in the ability of IP6 to antagonize the angiogenic and mitogenic activity of FGF1.

Angiogenesis is a biological phenomenon involving the growth of new blood vessels from preexisting vessels and is considered as a fundamental process in the development, progression, and metastatic spread of solid tumors (*1*, *2*). FGFs (fibroblast growth factors) are known to possess angiogenic and lymphangiogenic abilities. FGF1[1] (acidic fibroblast growth factor) and FGF2 (basic fibroblast growth factor) consisting of 155 and 154 amino acids, respectively, are considered as the prototype of FGFs; thus these two proteins are considered as paradigms for the entire FGF family (*3*−*5*). FGF1 and FGF2 are two of the most important angiogenesis-promoting polypeptides in the FGF family of mitogens. Besides facilitating angiogenesis, they also regulate a wide array of important biological processes, such as cellular differentiation, diabetic retinopathy, rheumatoid arthritis, atherosclerosis, tumor growth, neurogenesis, and embryogenesis (*6*−*8*). FGFs mediate cellular functions by binding to fibroblast growth factor receptors, which are known as protein tyrosine kinases, at the cell surface (*9*). FGFs are known for their dependence on heparin in order to induce their mitogenic activity and are found either bound to heparin or heparin sulfate in the extracellular space (*4*, *5*, *10*). In addition to FGFs, VEGF (vascular endothelial growth factor) is another important family of signal proteins that are involved in the stimulation of the growth of new blood vessels (*1*, *2*, *6*). They are also activated by binding to its receptor.

Three-dimensional structures of the free FGF1 and free FGF2 proteins were initially determined by X-ray crystallography (*11*). Both the FGF1 and FGF2 have similar molecular folds consisting of 12 antiparallel β-strands arranged in a pattern with approximate 3-fold internal symmetry. β-Strands β-1, β-4, β-5, β-8, β-9, and β-12 form a six-stranded antiparallel β-barrel that is closed at one end by a β-sheet interaction involving strands β-2, β-3, β-6, β-7, β-10, and β-11. Extended loops occur between strands β-3 and β-4, β-7 and β-8, and β-11 and β12. FGF1 and FGF2 are structurally (β-trefoil) homologous to IL-1β and soybean trypsin inhibitor (*12*, *13*). Structural studies of FGFs and its corresponding complexes with heparin and synthetic hexasaccharide heparin analogues (*14*−*16*), antiulcer agents such as sucrose octasulfate (SOS), and polyanions such as myoinositol hexasulfate (MIHS) in addition to heparin-like hexasaccharides have been reported (*17*−*20*). It has been indicated from these X-ray crystal and NMR structural studies that the heparin binding region of FGFs is located near to the loops of the β-10 and β-11 and of the β-11 and β-12 strands in C-terminal region. All of these structural studies stressed on the activation of the inherent mitogenic activity in FGF, while the other studies included the inhibition of the mitogenic/angiogenic activity of the FGFs. The crystal structure of FGF1 in complex with 5-amino-2-naphthalenesulfonate and the antiangiogenic compound 1,3,6-naphthalenetrisulfonate (NTS) were also reported (*3*, *21*). However, these compounds were substantially not effective enough to inhibit the inherent biological activity of FGFs. At higher concentrations of heparin, NTS was found to be ineffective like another compound suramin, as reported previously (*22*−*24*).

[†]We acknowledge financial support from the National Science Council (NSC) Taiwan (Grant NSC 98-2113-M-007-018-MY2).

[‡]The molecular coordinates are deposited in the PDB with entry 2k8r, and the NMR data are deposited in the BMRB with an entry number of 15960.

*Address correspondence to this author. Fax: 011-886-35-711082. Phone: 011-886-35-721524. E-mail: cyu.nthu@gmail.com.

[1]Abbreviations: FGF1, acidic fibroblast growth factor; VEGF, vascular endothelial growth factor; IP6, inositol hexaphosphate; NMR, nuclear magnetic resonance; HSQC, heteronuclear single-quantum coherence spectroscopy; TOCSY, total correlation spectroscopy; NOE, nuclear Overhauser effect; NOESY, nuclear Overhauser enhancement spectroscopy; ITC, isothermal calorimetry; CD, circular dichroism; ARIA, ambiguous restraints for iterative assignment; CNS, crystallography and NMR system; rmsd, root-mean-square deviation.

 Published on Web 11/15/2010

Inositol hexaphosphate (IP6) acts as an antagonist to fibroblast growth factor due to inhibition of its receptor binding ability (*25*). IP6 has been shown to exhibit antiangiogenic activity through analysis of the matrigel assay (*26*). In addition, IP6-mediated inhibition of FGF1 binding to cell surface receptors was first demonstrated in HepG2 cells (*25*). Interestingly, IP6 is a naturally occurring polyphosphorylated cyclitol and is present in high concentrations (0.4−6.4%) in corns, cereals, nuts, and high fiber-content foods (*27*). In addition to the presence of IP6 in plants, IP6 is also found in small quantities in practically all mammalian cells. Furthermore, IP6 involvement in signal transduction pathways has been shown to affect cell cycle regulation, growth, and differentiation of malignant cells (*28*, *29*), and its anticancer properties have been demonstrated in various experimental models (*30*). IP6 is recognized as a strong physiological antioxidant (*31*) that facilitates the control of tumor growth. In addition, IP6 was shown to have a synergistic effect in combination with other antiangiogenic agents as indicated by a marked enhancement in its antiangiogenic activity (*26*). Besides its anticancer properties, IP6 is beneficial to human health for its ability to enhance the immune system by augmenting the carcinogen-induced suppression of natural killer cell activity *in vivo* (*32*).

Detailed knowledge of the structural basis of protein function is important for the development of pharmacological agents for the treatment of human diseases. FGFs are potentially involved in a wide variety of human pathologies. The present study aims to increase the understanding of the interactions between FGF1 and IP6 at the molecular level. Herein, we used a variety of biophysical methods including isothermal calorimetry (ITC), CD spectrometry, and multidimensional NMR to characterize the interactions between FGF1 and IP6.

MATERIALS AND METHODS

Reagents. Heparin−Sepharose column were purchased from Amersham Pharmacia Biotech. Labeled NH_4Cl (^{15}N), labeled glucose (^{13}C), and D_2O were purchased from Cambridge Isotope Laboratories. The components for the Luria broth media were obtained from AMRESCO. Aprotinin, pepstatin, leupeptin, phenylmethanesulfonyl fluoride, Triton X-100, β-mercaptoethanol, and inositol hexaphosphate (IP6) were all purchased from Sigma Co. (St. Louis, MO). The Centricon and Amicon membranes were purchased from Millipore. All of the other chemicals used in the study were of high quality analytical grade.

Protein Expression and Purification. The recombinant human FGF1 clone was inserted into the pET20 vector and was overexpressed in the *Escherichia coli* BL21(DE3) strain as described previously (*33*). The overexpressed protein was then purified using a heparin−Sepharose column and eluted with a linear NaCl gradient (0−1.5 M). The protein was desalted by ultrafiltration using an Amicon apparatus. The homogeneity of the FGF1 protein was determined using SDS−polyacrylamide gel electrophoresis. The protein concentration was then estimated using a UV spectrophotometer by measurement of the OD at 280 nm.

Preparation of the ^{15}N- and ^{13}C-Labeled FGF1. The uniform labeling of FGF1 using isotopes ^{15}N and ^{13}C was achieved using M9 minimal medium. This medium contained either $^{15}NH_4Cl$ for single (^{15}N) labeling or $^{15}NH_4Cl$ and [^{13}C]glucose for double (^{15}N and ^{13}C) labeling of FGF1. The maximum expression yield was achieved using a modified M9 medium that included additional vitamins. The host expression strain, *E. coli* BL21(DE3)pLysS, is a vitamin B_1-deficient host, and therefore thiamin (vitamin B_1) was added in order to achieve yields up to 25−30 mg/L of the isotope-enriched medium.

For all of the NMR experiments involving the FGF1−IP6 complex, the sample was prepared with the protein at a concentration of approximately 17 mg/mL (1 mL) and was diluted approximately 10 times with a buffer composed of 25 mM phosphate (pH 6.8) and 100 mM ammonium sulfate. Inositol hexaphosphate (2 mM) was added to the sample, which was then concentrated to 0.5 mL in a procedure that was repeated three times until a final concentration of 1.5 mM was achieved for 3D NMR experiments or 1 mM for 2D NMR experiments.

Isothermal Calorimetry (ITC) Experiment. A VP-ITC titration calorimeter (MicroCal, Inc., Northampton, MA) was used for the study. The protein (FGF1) was incubated in buffer composed of 25 mM phosphate (pH 6.8) and 100 mM ammonium sulfate. A protein concentration of 0.1 mM was used for the ITC titration experiment. The protein and ligand samples were degassed under vacuum before the titration. After equilibration at 25 °C, the protein was contained in the sample cell to which IP6 at a concentration of 2 mM was injected in 30 × 8 μL aliquots using the default injection rate of 240 s time interval between two successive injections. The raw ITC data were corrected for the heat of dilution of the titrant. The analysis of the ITC experiments was carried out by the software supplied by the VP-ITC microcalorimeter.

CD Measurements. Circular dichroism measurements (CD) were collected using an AVIV CD spectrophotometer for determination of thermal stability. The thermal denaturation curves of the native free FGF1 and of the FGF1−IP6 complex were performed over a temperature range of 25−79 °C at intervals of 3 °C for each data set in order to determine the T_m of the protein in the presence and absence of ligand. The protein sample was present in 25 mM phosphate buffer (pH 6.8) containing 100 mM ammonium sulfate. Typically the concentration of the protein was 4 μM, and that of the FGF1−IP6 complex was a 1:1 ratio of protein to IP6. The CD spectrum of the free FGF1 shows a positive ellipticity band at 228 nm, which is characteristic of a β-barrel protein, while the protein in the denatured state shows the complete loss of the 228 nm CD band. The ΔG of unfolding was calculated based on the slope of the folded and unfolded state baseline (*34*).

NMR Experiments. All of the 2D and 3D NMR resonance experiments were performed using a Bruker Avance-600 MHz NMR spectrometer equipped with a cryoprobe and were performed at 25 °C. For the 2D NMR experiments the concentration of the protein used was 1.0 mM, and for the 3D NMR experiments a protein concentration of 1.5 mM was used. The backbone assignments of the IP6-bound FGF1 amide protons were identified based on the assignments of the free FGF1 $^1H-^{15}N$ HSQC; however, some of the residues that were difficult to distinguish in the 2D HSQC were identified through subsequent 3D HNCA (*35*) experiments. In addition, the C^α and C^β carbon resonances were identified by CBCA(CO)NH (*36*) experiments while the carbon side chain of the protein binary complex was resolved by a CC(CO)NH (*37*) experiment. Furthermore, the presence of a carbonyl carbon was determined by the HNCO (*38*) experiment, and the α and β proton side chain resonances were resolved by performing the HBHA(CO)NH (*36*) experiment. The proton side chains were assigned from the NMR data obtained from HCCH-TOCSY (*39*) experiments and from

^{15}N-edited TOCSY-HSQC (*40*). The three-dimensional ^{13}C-edited NOESY and ^{15}N-edited NOESY (*41*) spectra of uniformly ^{13}C/^{15}N-labeled protein were acquired with a mixing time of 100 ms. In addition, in the ^{13}C(ω_2)-edited ^{12}C(ω_3)-filtered NOESY (*42*) experiment, the spectrum of the complex form of the protein was acquired in 100% D_2O with a mixing time set to 120 ms. All of the spectra were processed using Topspin and analyzed with the Sparky software (*43*). The cross-peaks in the ^{15}N-edited NOESY-HSQC and ^{13}C-edited NOESY-HSQC spectra were manually picked using Sparky, and the volume of the integrated peaks was used for structure calculation. The H/D exchange experiment is detailed in Supporting Information.

NMR Titration Experiment and Calculation of the Binding Constant. Titration of the ^{15}N-labeled FGF1 with IP6 was used in order to determine the protein residues that are involved in ligand binding by measuring the changes in the amide proton and nitrogen chemical shifts via analysis of the 2D ^{1}H−^{15}N HSQC spectrum. A plot of the weighted average of the chemical shift perturbation (^{1}H and ^{15}N) was calculated using the equation

$$\Delta\delta = [(\delta^{1}\mathrm{HN})^2 + 0.2(\delta^{15}\mathrm{N})^2]^{1/2} \quad (1)$$

where δ^{1}HN and δ^{15}N represent the chemical shift perturbation values of the amide proton and nitrogen, respectively.

In order to evaluate the titration experiments of the ^{15}N-labeled FGF1 with IP6, the chemical shift perturbations of residues that were significantly affected were plotted as a function of the ligand concentration. A minimum of six different protein:ligand ratios were analyzed for the interaction, ranging from 1:0.1 to 1:2. In addition, ^{1}H−^{15}N HSQC spectra were obtained after each addition, and the chemical shift of each amide resonance was measured. The dissociation constant of FGF1 and IP6 was evaluated by the titration experiments of the ^{15}N-labeled FGF1 protein with IP6, and the chemical shift values (^{1}H and ^{15}N) of significantly affected residues were plotted against the ligand concentration and the binding constant determined based on the equation (*44*)

$$\Delta = \Delta_0 \frac{(K_d + [L] + [P]) - \sqrt{(K_d + [L] + [P])^2 - 4[P][L]}}{2[P]} \quad (2)$$

where Δ is the observed change in the chemical shift, Δ_0 is the total change in chemical shift at saturation, and [L] and [P] are the ligand and protein concentrations, respectively.

Structure Calculations. Structure calculations were performed using ARIA/CNS (*45*). We used a variety of triple resonance NMR experiments to solve the solution structure of FGF1 in the FGF1−IP6 complex.

Interproton distance constraints were derived from the ^{13}C-edited NOESY and ^{15}N-edited NOESY spectrum. All of the NOEs were grouped into three distance ranges, 1.8−2.9, 1.8−3.5, and 1.8−5.0 Å, corresponding to short-, medium-, and long-range NOEs, respectively. In addition, information regarding the hydrogen bonds was derived from the hydrogen−deuterium exchange experiment while dihedral angle restraints were generated using TALOS (*46*) with the HN, CA, CO, and HA. A total of 200 structures were calculated and further refined with CNS in an explicit solvent layer of water from which the best 20 structures with the lowest energy were selected. The calculated structures of the protein were analyzed with PROCHECK in order to extract structural parameters. MOLMOL and PYMOL were then used for structural representation.

Molecular Docking. The FGF1−IP6 complex was determined using the docking program HADDOCK (High Ambiguity Driven DOCKing) (*47*, *48*) in combination with CNS (*49*). The IP6 coordinates were taken from the PDB. The topology and the parameter files were generated using the HIC-UP server (*50*). The docking procedure was driven based on the intermolecular NOE data derived from the ^{13}C(ω_2)-edited ^{12}C(ω_3)-filtered NOESY experiment. The qualitative distance restraints (4.0−6.0 Å) were used to dock IP6 with the ARIA/CNS derived structure of FGF1. The intermolecular data were provided as unambiguous restraints. The residues that showed higher chemical shift perturbations in the FGF1−IP6 complex were used to define the ambiguous interaction restraints (AIRs). Depending on the solvent accessibility, from the PDB structure of FGF1 in complex with IP6, these AIRs were determined either as active or passive residues. Active residues are those residues whose solvent accessibility is larger than 50% while the passive residues are those whose solvent accessibility is less than 50%. We used NACCESS (*51*) in order to determine the solvent-exposed residues in FGF1.

The docking calculations were performed using HADDOCK 2.0 where the FGF1 (calculated from ARIA/CNS) and the IP6 parameters were optimized using PARALLELHDG, which included the optimized potentials for liquid simulation (OPLS) parameters for nonbonded interactions (*52*). A total of 4000 structures were calculated, and the 50 structures obtained after water refinement were analyzed. The FGF1−IP6 binary complex structures were selected based on the structures with lowest energy conformers.

Cell Growth Assay. The MCF-7 cell line was used for studying the cell proliferation in the presence or absence of FGF1/heparin/IP6, and the relative cell numbers were determined by WST-1 reagent (Roche). MCF-7 cells were plated overnight at a density of 10000 cells/well in 96-well plates and subsequently incubated in serum-free medium containing 0.1% BSA for 24 h. Serum-starved cells were treated with 5 ng/mL FGF1 in the absence and presence of heparin or treated with indicated concentrations of IP6 in the presence of 5 ng/mL FGF1 and 5 μg/mL heparin for another 48 h. The relative cell numbers were determined by WST-1 reagent (Roche) according to the instruction. One-tenth volume of WST-1 was added into each well, the plates were incubated for 4 h, and then the absorbance was measured at 450 nm and reference wavelength at 650 nm by using a microplate reader.

RESULTS

Chemical Shift Perturbation Experiments. In the present study, we used a truncated form of FGF1 consisting of 133 amino acids that has equivalent biological activity to the full-length FGF1 protein (*18*). The ^{1}H−^{15}N 2D HSQC spectrum provides a fingerprint of the conformational states of a particular protein. The cross-peaks of the spectrum represent the chemical environment of the backbone and side chain amides of the protein. The overlaid ^{1}H−^{15}N HSQC spectra of the free FGF1 and the FGF1−IP6 binary complex provide information regarding the amino acid residues of FGF1 that interact with IP6. A significant chemical shift perturbation was observed in the overlap of the ^{1}H−^{15}N HSQC spectra of the free FGF1 with the FGF1−IP6 complex titrated at 1:1 ratio (Figure 1a). The chemical shift

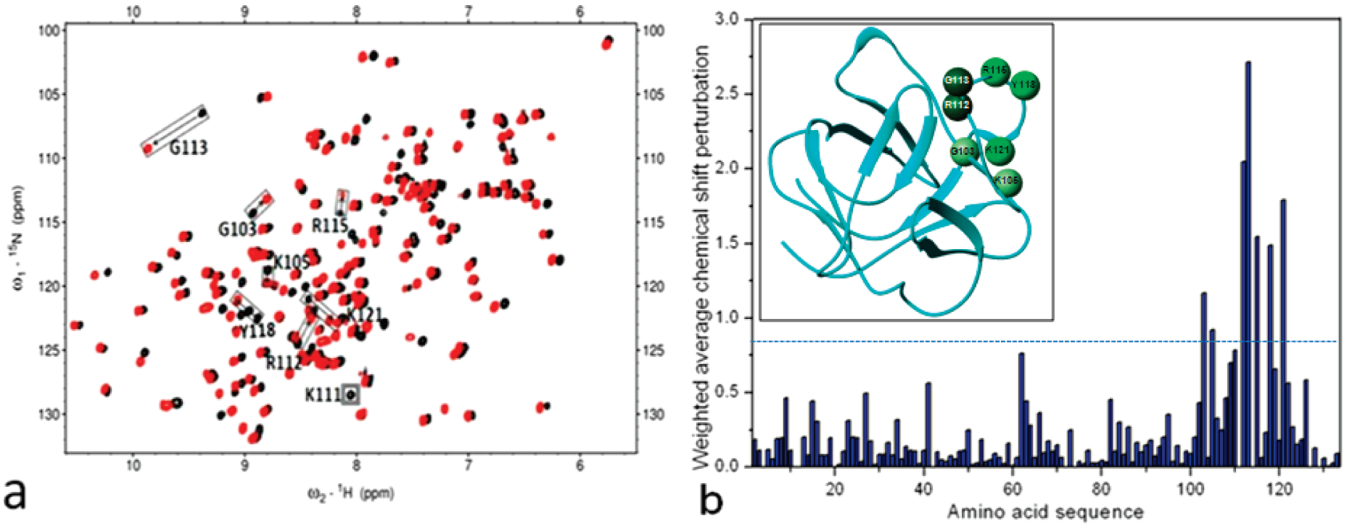

FIGURE 1: Analysis of the free FGF1 and FGF1−IP6 complex using 2D NMR at a 1:1 ratio. (a) The overlaid 2D [^{1}H−^{15}N] HSQC spectra highlight the spectral changes of the uniformly ^{15}N-labeled FGF1 (unbound, black) and FGF1 upon binding to IP6 (binary complex, red). The residues showing maximal perturbation in the chemical shift upon binding to the ligand are indicated by arrows, and the cross-peak that disappeared (corresponding to K111) is boxed. (b) The weighted average of the chemical shift (^{1}H and ^{15}N) perturbations $\{\Delta\delta = [(\delta^1\mathrm{HN})^2 + 0.2(\delta^{15}\mathrm{N})^2]^{1/2}\}$ of the amino acid residues in FGF1 upon complex formation with IP6 are represented as a bar diagram. The residues that are not indicated in the bar diagram include proline residues or the residue whose shifts were not measured upon overlap. The inset depicts the significant chemical shift perturbed residues mapped over the ribbon diagram of the FGF1 structure.

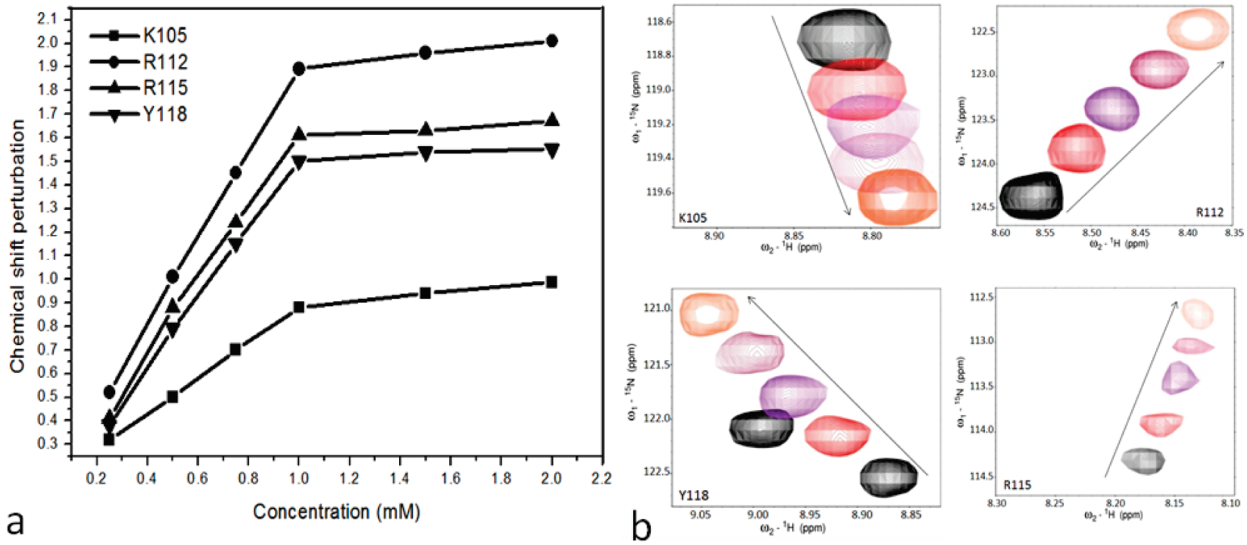

FIGURE 2: Chemical shift perturbation of the ^{15}N-labeled FGF1 amino acid residues during the NMR titration with increasing concentration of IP6. (a) NMR titration curves for the FGF1 residues K105, R112, R115, and Y118 with increasing concentration (0, 0.25, 0.5, 0.75, 1, 1.5, and 2 mM) of IP6. Overall six data points were collected and plotted in the graph. (b) The regions of the 2D [^{1}H−^{15}N] HSQC spectra showing the movement of the cross-peak of the FGF1 residues in the FGF1−IP6 complex (K105, R112, R115, and Y118) that show the chemical shift perturbation at various concentrations of ligand (0, 0.25, 0.5, 0.75, 1 mM; the cross-peak shifts are indicated as the IP6 concentration increases).

perturbations observed in the bound form of FGF1 might also arise as a result of local conformational rearrangement that could be indirectly prompted by IP6 binding. Upon titration of FGF1 and IP6 in 1:1 ratio, it could be noted that some of the residues of FGF1 have shown chemical shift perturbation higher than 0.5 ppm while residues G103, K105, R112, G113, R115, Y118, and K121 showed higher chemical shift perturbation (Figure 1b). The region showing higher chemical shift perturbation was considered as the putative binding region of IP6. The cross-peak of K111 residue disappeared at this ratio due to line broadening.

The comparison of the weighted average of the chemical shift values in the free protein to those of the bound protein to estimate the corresponding weighted average changes ($\Delta\delta$) proved to be a useful method for elucidating the protein−ligand binding interface (*16*, *53*). The maximum chemical shift perturbation (eq 1; see Materials and Methods) observed in the FGF1−IP6 complex was more than 2.5 ppm. The dissociation constant (K_d) between FGF1 and IP6 was determined based on the analysis of the ^{1}H−^{15}N HSQC spectrum of FGF1 plotted as a function of increasing concentration of IP6 (Figure 2a). The cross-peaks corresponding to each residue were traced by the addition of increasing concentrations of IP6 to the free FGF1 (Figure 2b). A curve fit with eq 2 (see Materials and Methods) using the chemical shift perturbation from the significantly perturbed cross-peaks indicated a dissociation constant in the range of 13−25 μM. The cross-peaks that shifted upon addition of

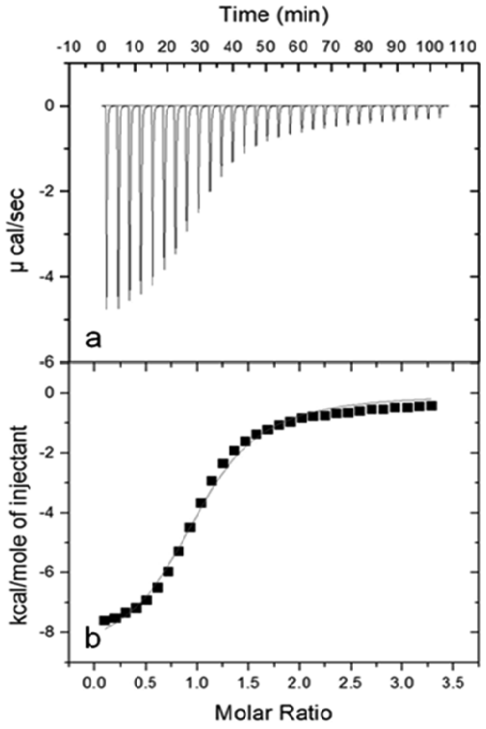

FIGURE 3: Isothermogram representing the heat change during the titration of IP6 with FGF1. (a) The raw data of the titration of the FGF1 with IP6. (b) The integrated data obtained from the raw data (MicroCal software).

increasing concentration of IP6 showed no further significant shift after FGF1 and IP6 was titrated to 1:1 ratio.

H/*D Exchange*. In the H/D exchange experiment, the amide protons in FGF1 were monitored using NMR spectroscopy. Based on the accessibility to the solvent, the amide hydrogen could exchange with deuterium to result in disappearance of the residual cross-peak in $^{1}H-^{15}N$ HSQC spectra. The hydrogen−deuterium exchange could range from fast to slow exchange. The slow H/D exchange is signified by an increase in the amide proton lifetime. Initially, we confirmed the binding site of IP6 on FGF1 by monitoring the amide proton occupancy of the residues showing higher chemical shift perturbation. We compared the H/D exchange rates of the free form of FGF1 and the IP6-bound form of the FGF1 by analyzing $^{1}H-^{15}N$ HSQC spectra at different time intervals. The comparison of the amide proton occupancy of residues K105, S109, and K121 in the free FGF1 and FGF1−IP6 complex is shown in Supporting Information Figure S1.

Isothermal Calorimetry (*ITC*). The ITC experiment was successfully used to evaluate the binding affinities and enthalpy of binding reactions in solution and also to characterize the binding of the small molecules to proteins (*54*, *55*). From the data obtained, a single binding site model was used for fitting the curve in the Microcal software to characterize the binding affinities and enthalpy and entropy of the reaction (Figure 3). The ΔH value was −8.9 kcal mol^{-1}, and the ΔS was −7.83 J K^{-1}. Both the observed enthalpy and entropy are negative values, and this binding can be characterized by a large and favorable enthalpy of binding that is partly offset by an unfavorable entropy term. Most of the antigen−antibody complexes belong to this category of binding (*56*, *57*), and the thermodynamic behavior has been attributed to charge−charge, van der Waals, and hydrogen-bonding interactions (*58*, *59*). The dissociation constant (K_d) value was determined as 16 μM; this value is in good agreement with the calculated dissociation constant obtained from 2D NMR $^{1}H-^{15}N$ HSQC titrations.

Table 1: Structural Statistics of FGF1 in the FGF1−IP6 Complex from the ARIA/CNS Structure Calculation of the 20 Best Conformers

Distance constraints (Å)	
long range	361
medium range	101
short range	326
intraresidue [$i = j$]	362
dihedral angle constraints (φ and ψ)	124
hydrogen bond constraints	41
Average rmsd to the mean structure (Å)	
residues 3−130	
backbone atoms	0.9 ± 0.16
heavy atoms	1.8 ± 0.17
regular secondary structure elements	
backbone atoms	0.7 ± 0.10
heavy atoms	1.4 ± 0.15
deviations from idealized geometry	
bond lengths (Å)	0.006 ± 0.0002
bond angles (deg)	0.485 ± 0.013
impropers (deg)	0.215 ± 0.017
Procheck *G*-factors	
dihedrals	−0.36
covalent	0.65
overall	0.03
Ramachandran statistics (% of all residues)	
most favored	72.6
additionally allowed	23.0
generously allowed	3.5
disallowed	0.9

FGF1 Is Stabilized by the Binding of IP6. The conformational changes that occur during the process of thermal denaturation in a protein are determined by circular dichroism (CD) technique. The thermal denaturation of the free FGF1 and IP6-bound form of FGF1 was analyzed separately at temperatures ranging from 25 to 79 °C. Upon comparison and analysis of the CD data, indicated by the positive ellipticity band at 228 nm (characteristic of a protein possessing a β-barrel), the T_m (temperature at which 50% of the protein is in the native form) of the protein increased by 4 °C in the IP6-bound form of FGF1 (Supporting Information Figure S2), indicating that IP6 stabilizes FGF1 thermodynamically upon complex formation. The free energy of the FGF1 protein is 6.2 kcal mol^{-1}, and the free energy of the FGF1 in the FGF1−IP6 complex is 8.4 kcal mol^{-1}. The unfolding free energy of FGF1 increased 2.2 kcal mol^{-1} in the presence of IP6.

DISCUSSION

Solution Structure of the FGF1 in the FGF1−IP6 Complex. We have determined the solution structure of the FGF1 in the FGF1−IP6 complex using multidimensional NMR spectroscopy. The backbone assignments of the IP6-bound FGF1 amide protons were identified based on the assignments of the free FGF1 $^{1}H-^{15}N$ HSQC. More than 95% of ^{1}H, ^{15}N, and ^{13}C chemical shifts were assigned in this set of analyses. All of the amide protons of the amino acid residues were assigned with the exception of the K111 residue that could not be resolved in the binary complex from the $^{1}H-^{15}N$ HSQC spectrum. However, its corresponding C^{α}, C^{β}, and proton side chain were assigned through HNCA, CBCACONH, HBHA(CO)NH, and HCCHTOCSY experiments. The aromatic resonances were

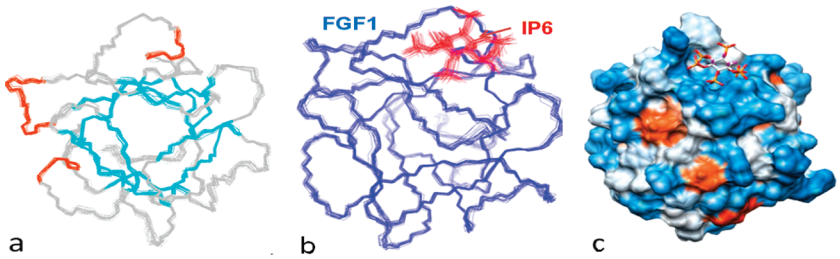

FIGURE 4: Solution structure of the FGF1−IP6 complex. (a) An overlay of 20 structures showing the backbone representation of the FGF1 in the FGF1−IP6 complex. In the structured region the cyan color represents the 12 β-sheets, the red color represents α-helix, and the loop region is represented in gray. (b) An overlay of 20 structures of the FGF1 in complex with the IP6 structure. IP6 is shown in red; FGF1 is shown in blue. (c) The electrostatic representation of the FGF1−IP6 complex.

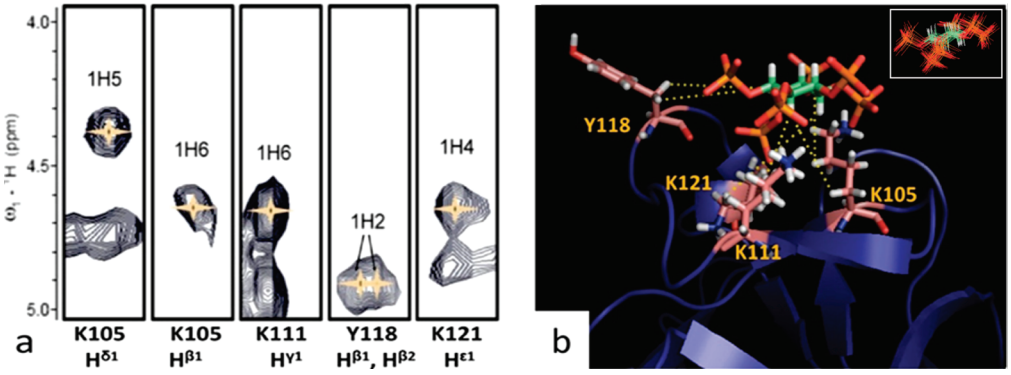

FIGURE 5: Intermolecular NOEs between FGF1 and IP6. (a) The intermolecular NOE peaks of the FGF1−IP6 complex were observed in the $^{13}C(\omega_2)$-edited $^{12}C(\omega_3)$-filtered NOESY experiment and are represented in strips. The corresponding protons of the FGF1 and IP6 are labeled in strips. (b) A magnified view of the FGF1−IP6 complex showing the binding region and the corresponding residues involved in binding are labeled in the figure. The side chains of the aforementioned residues and the intermolecular interactions between FGF1 and IP6 are represented using dotted lines. An ensemble of 20 IP6 structures is shown in the inset.

confirmed using the ^{13}C-edited NOESY experiment. In addition, the NH_2 groups of the Gln and Asn amino acid residues were correlated to their H^{β} and H^{α} protons by the 3D ^{15}N-edited NOESY experiment.

The structure of FGF1 in the FGF1−IP6 complex was determined by ARIA/CNS. Distance restraints were subsequently generated from the ^{15}N-edited NOESY-HSQC spectrum and ^{13}C-edited NOESY-HSQC spectrum and used for the structure calculation. In addition, hydrogen bond restraints in the FGF1 of the FGF1−IP6 complex derived from the H/D exchange experiment were also used for the structure calculation. The structural restraints and statistics of the ensemble of the NMR structures of FGF1 in the FGF1−IP6 complex calculated by ARIA/CNS are represented in Table 1. According to Ramachandran analysis, 72.6% of the residues are in the most favored region, and less than 0.9% of the residues are in the disallowed region. The solution structure of the FGF1 in the FGF1−IP6 complex shows 12 β-sheets arranged in β-trefoil architecture (Figure 4a). Figure 4b represents backbone overlap of 20 FGF1−IP6 complex structures, and Figure 4c represents the electrostatic representation of the FGF1−IP6 complex. The calculated structure of the FGF1 in the FGF1−IP6 binary complex overlaps with the crystal structure of free FGF1 (PDB: 1RG8) in the secondary structured region (12 β-sheets) with a backbone rmsd of 1.4 Å (Supporting Information Figure S4).

In order to determine the complex structure of FGF1 with IP6, we used the intermolecular NOEs and ^{1}H−^{15}N HSQC chemical shift perturbation data. The FGF1−IP6 binary complex was resolved using the docking program HADDOCK. The active and passive residues for the HADDOCK calculations included residues K105, R115, Y118 and residues G103, R112, G113, and K121, respectively, all of which were in the IP6 binding region of FGF1. Six intermolecular NOEs were used for the complex structure calculation which were observed with the residues K105, K111, Y118, and K121 in the FGF1−IP6 binary complex (Figure 5a). These intermolecular NOEs are illustrated in Figure 5b. The other amino acid residues in the IP6 binding region (G103, R112, G113, and R115) showed a significant chemical shift perturbation; however, no intermolecular NOEs were observed with these residues. It is interesting to note, as reported previously by Maciag et al., that mutation of amino acid residue G103 drastically lowered the mitogenic activity of the protein (*10*). Mutations of the lysine residues in this region (amino acid residues 103−111) can also have significant yet varying effects on the ability of FGF1 to bind heparin. Additional site-directed mutagenesis studies indicated that mutation of lysine residues 105, 106, or 111 resulted in the most significant reduction in the apparent binding affinity of FGF1 for heparin (*60*). Some of these amino acid residues are involved in IP6 binding.

Description of the FGF1−IP6 Binding Region. The region K105−K121 in FGF1 is characterized by a significant amount of positively charged residues that can be attributed to the side chains of the amino acids such as lysine and arginine shown in blue color (Figure 4c). The residues that showed the maximum chemical shift perturbation were observed in this region. In the present study we have identified that IP6 binds to the side chains of the positive amino acid residues K105, K111, and K121 in addition to residue Y118 of FGF1. Mainly charge−charge interactions are involved in the formation of the FGF1−IP6 complex. IP6 has differentially oriented phosphates (5 equatorial, 1 axial). In the FGF1−IP6 complex structure the phosphate on the second carbon which is

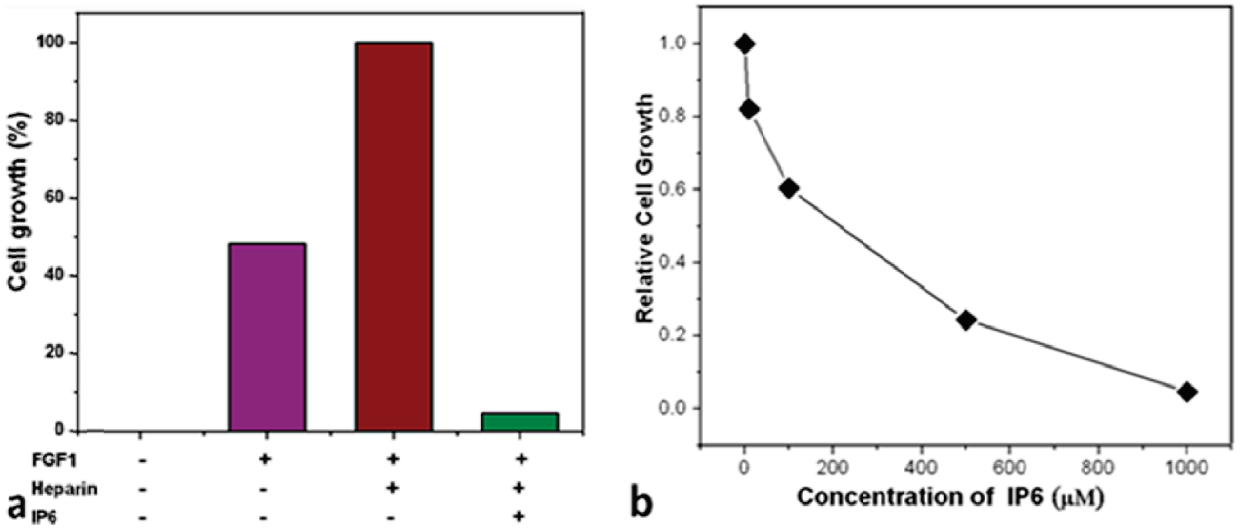

FIGURE 6: Effect of IP6 on inhibition of mitogenic activity in FGF1. Each panel is representative of the average of six separate experiments. (a) The inhibitory effects of IP6 on the FGF1 mitogenic activity was assessed by exposure to the MCF-7 cell line. IP6 suppresses the mitogenic activity in FGF1 to about 95%. (b) Serum-starved MCF-7 cells were supplemented with FGF1 (5 ng/mL) and heparin (5 μg/mL) and treated with different concentrations of IP6 (0−1000 μM). A dose−response showing the downregulation of FGF1 mitogenic activity was observed.

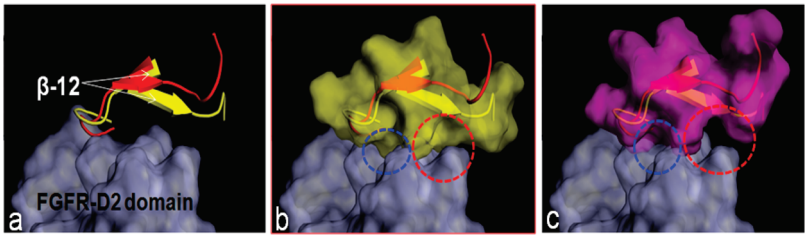

FIGURE 7: An illustration of the binding interface region between the FGF1 and FGFR-D2 domain. (a) The β-12 strand of the active form (PDB: 1E0O) of FGF1 and surface diagram of the FGFR-D2 domain is represented in yellow and cyan color, respectively. The β-12 strand of the FGF1−IP6 structure shown in red color is overlapped with FGF1 of the active form. The orientation of the FGF1 structure of the FGF1−IP6 binary complex (Red) was oriented away from the interface with the FGFR-D2 domain. (b) Surface representation of the active form of the FGF1 structure (PDB: 1E0O). The β-12 strand (yellow) indicates regions of contact shown in blue and red dotted circle. (c) Surface representation of the β-12 strand (red) of the FGF1−IP6 complex is shown in magenta. The area of contact of FGF1−IP6 is disrupted at its interface region with the FGFR-D2 domain. The differences in the topology at the interface of the FGF1 and FGFR-D2 domain are clearly displayed in panels b and c.

equatorial was oriented near to the R115 and Y118 residues. The side chain NH2 of R115 is hydrogen bonded to IP6 O21, O32, O33 oxygen whereas hydrogen bonds were also observed with the backbone amide protons of K111 and G119 with O22 and O43 oxygen of IP6, respectively.

Cell Growth Assay. IP6 was previously shown to be an antagonist for FGF−FGFR-induced mitogenesis. In order to determine whether heparin and IP6 modulate the mitogenic effects of FGF1, cells were grown under serum-free medium and then treated with FGF1 without or with heparin and IP6. FGF1 enhanced the growth of MCF-7 cells, and heparin significantly facilitated the effects (Supporting Information Figure S5). We further examined the effects of IP6 on FGF1-enhanced cell growth. IP6 suppressed the cell growth at the concentration from 100 to 1000 μM in a dose-dependent manner (Figure 6). In particular, the cell growth reduced to the level of untreated cells after the treatment of 1000 μM IP6, indicating that IP6 effectively competed the effect of heparin on FGF1. Thus, IP6 is a potent compound to inhibit the growth of FGF1-responsive cells, indicating its effective role in cell signaling. The growth of cells in the absence of FGF1, heparin, and IP6 was taken as the negative control with 0% growth, and the presence of FGF1 (5 ng/mL) and heparin (5 μg/mL) was taken as the positive control showing 100% cell growth.

Mechanism of Inhibition of FGF1−FGFR Receptor Binding by IP6. Acidic fibroblast growth factor is known to possess angiogenic properties and is also known to be involved in the progression of various tumors. Previous reports focused on the heparin-induced activation of FGF as a prerequisite to bind to the FGF receptor (FGFR) for inducing its inherent mitogenic activity (*61*−*64*). Other molecules like MIHS and SOS (*18*, *19*) were also reported to bind to FGF1 and activate like heparin for the mitogenic activity. However, IP6 is an antagonist against FGFR (receptor) binding and is involved in antiangiogenic activity. IP6 inhibited the growth of the endothelial cells whereas MIHS has no effect on the growth of either endothelial cells or epithelial cells, indicating the specific effect of IP6 (*25*, *26*). Our results on cell growth assay indicated that IP6 inhibits the cell proliferation in the FGF1-responsive cells, indicating its effective role in cell signaling (Figure 6).

Previously, it was reported that the truncation of the N- and C-terminal amino acids does not affect the three-dimensional structure of FGF1 (*65*); however, their elimination has a significant decrease in the mitogenic activity (*66*, *67*). Thus it is evident that these N- and C- terminal regions play a prominent role in the mitogenic activity of FGF1. As reported earlier the conformational change in FGF1 at the NTS binding region was known to hinder the FGF1 mitogenic activity to a certain extent;

however, the effect was nullified by the addition of heparin (*3*). Herein our results indicated conformational changes in the tertiary structure of FGF1 in the FGF1−IP6 complex which included the ligand binding region and also the C-terminal region (Figure 7). Upon comparison with the earlier reported crystal structure of the FGF1−FGFR−heparin complex structure (PDB: 1E0O) with the FGF1 structure in the FGF1−IP6 binary complex, we found differences in the orientation of the β-12 strand region of FGF1 which was oriented away from the FGFR−D2 receptor binding interface (Figure 7a). It was also noticed that the β-12 strand of the FGF1 in the FGF1−IP6 complex was buried inside and was less accessible to FGF receptor binding at the interface when compared to the heparin-bound active form of FGF1 (PDB: 1E0O). The surface representation of Figure 7b,c revealed that the FGFR−D2 receptor binding interface region of FGF1 in the FGF1−IP6 complex was disrupted.

In this report, we have elucidated the structural interactions between FGF1 and IP6 and provided the mechanistic insight as to how IP6 could act as an antagonist to FGF-FGFR signaling. The results indicate IP6 binding to FGF1 brings about the structural changes in the protein and thus can prevent the interaction between FGF1 and FGFR. Perhaps most importantly, the elucidation of the solution structure of the FGF1−IP6 binary complex could be useful for improving current antagonists or possibly designing better antagonists for FGF1. On the basis of the present results we are interested in studying the protein dynamics of the IP6-bound FGF1 complex.

SUPPORTING INFORMATION AVAILABLE

Hydrogen−deuterium exchange, analysis of thermal stability in FGF1 in the presence of IP6, and triple resonance NMR spectrum strips. This material is available free of charge via the Internet at http://pubs.acs.org.

REFERENCES

1. Folkman, J. (1971) Tumor angiogenesis: therapeutic implications. *N. Engl. J. Med. 285*, 1182–1186.
2. Folkman, J., and Klagsbrun, M. (1987) Angiogenic factors. *Science 235*, 442–447.
3. Lozano, R. M., Jimenez, M., Santoro, J., Rico, M., and Gimenez-Gallego, G. (1998) Solution structure of acidic fibroblast growth factor bound to 1,3,6-naphthalenetrisulfonate: a minimal model for the anti-tumoral action of suramins and suradistas. *J. Mol. Biol. 281*, 899–915.
4. Baird, A., and Bohlen, P. (1990) Fibroblast growth factors, in Handbook of Experimental Pharmacology, Peptide Growth Factors and Their Receptors (Sporn, M. B., and Roberts, A. B., Eds.) pp 369−418, Springer, Berlin.
5. Gimenez-Gallego, G., and Cuevas, P. (1994) Fibroblast growth factors, proteins with a broad spectrum of biological activities. *Neurol. Res. 16*, 313–316.
6. Folkman, J. (1995) Angiogenesis in cancer, vascular, rheumatoid and other disease. *Nat. Med. 1*, 27–31.
7. Beenken, A., and Mohammadi, M. (2009) The FGF family: biology, pathophysiology and therapy. *Nat. Rev. 8*, 235–253.
8. Powers, C. J., Mc Leskey, S. W., and Wellstein, A. (2000) Fibroblast growth factors, their receptors and signalling. *Endocr. Relat. Cancer 7*, 65–97.
9. Jaye, M., Schlessinger, J., and Dionne, C. A. (1992) Fibroblast growth factor receptor tyrosine kinases: molecular analysis and signal transduction. *Biochim. Biophys. Acta 1135*, 185–199.
10. Burgess, T., and Maciag, T. (1989) The heparin-binding (fibroblast) growth factor family of proteins. *Annu. Rev. Biochem. 58*, 575–602.
11. Zhu, X., Komiya, H., Chirino, A., Faham, S., Fox, G. M., Arakawa, T., Hsu, B. T., and Rees, D. C. (1990) Three-dimensional structures of acidic and basic fibroblast growth factors. *Science 251*, 90–93.
12. Murzin, A. G., Lesk, A. M., and Chothia, C. (1992) Beta-trefoil fold. Patterns of structure and sequence in the Kunitz inhibitors interleukins-1 beta and 1 alpha and fibroblast growth factors. *J. Mol. Biol. 223*, 531–543.
13. McLachlan, A. D. (1979) Three-fold structural pattern in the soya-bean trypsin inhibitor (Kunitz). *J. Mol. Biol. 133*, 557–563.
14. Faham, S., Hileman, R. E., Fromm, J. R., Linhardt, R. J., and Rees, D. C. (1996) Heparin structure and interactions with basic fibroblast growth factor. *Science 271*, 1116–1120.
15. DiGabriele, A. D., Lax, I., Chen, D. I., Svahn, C. M., Jaye, M., Schlessiner, J., and Hendrickson, W. A. (1998) Structure of a heparin-linked biologically active dimer of fibroblast growth factor. *Nature 393*, 812–817.
16. Canales-Mayordomo, A., Lozano, R., Lopez-Mendez, B., Angulo, J., Ojeda, R., Nieto, P. M., Martin-Lomas, M., Gimenez-Gallego, G., and Jimenez-Barbero, J. (2006) Solution NMR structure of a human FGF-1 monomer, activated by a hexasaccharide heparin analogue. *FEBS J. 273*, 4716–4727.
17. Blaber, M., DiSalvo, J., and Thomas, K. A. (1996) X-ray crystal structure of human acidic fibroblast growth factor. *Biochemistry 35*, 2086–2094.
18. Pineda-Lucena, A., Jimenez, M. A., Nieto, J. L., Santoro, J., Rico, M., and Gimenez-Gallego, G. (1994) ^{1}H-NMR assignment and solution structure of human acidic fibroblast growth factor activated by inositol hexasulfate. *J. Mol. Biol. 242*, 81–98.
19. Yeh, B. K., Eliseenkova, A. V., Plotnikov, A. N., Green, D., Pinnell, J., Polat, T., Linde, A. G., Linhardt, R. J., and Mohammadi, M. (2002) Structural basis for activation of fibroblast growth factor signalling by sucrose octasulfate. *Mol. Cell. Biol. 22*, 7184–7192.
20. Ogura, K., Nagata, K., Hatanaka, H., Habuchi, H., Kimata, K., Tati, S., Raveru, M. W., Jaye, M., Schlessinger, J., and Inagaki, F. (1999) Solution structure of human acidic fibroblast growth factor and interaction with heparin-derived hexasaccharide. *J. Biomol. NMR 13*, 11–24.
21. Fernandez-Tornero, C., Lozano, R. M., Redondo-Horcajo, M., Gomez, A. M., Lopez, J. C., Quesada, E., Uriel, C., Cuevas, P., Romero, A., and Gimenez-Gallego, G. (2003) Leads for development of new naphthalenesulfonate derivatives with enhanced antiangiogenic activity—Crystal structure of acidic fibroblast growth factor in complex with 5-amino-2-naphthalenesulfonate. *J. Biol. Chem. 278*, 21774–21781.
22. Middaugh, C. R., Mach, H., Burke, C. J., Volkin, D. B., Dabora, J. M., Tsai, P. K., Bruner, M. W., Ryan, J. A., and Marfia, K. E. (1992) Nature of the interaction of growth factors with suramin. *Biochemistry 31*, 9016–9024.
23. Pesenti, E., Sola, F., Mongelli, N., Grandi, M., and Spreafico, F. (1992) Suramin prevents neovascularization and tumor growth through blocking of basic fibroblast growth factor activity. *Br. J. Cancer 66*, 367–372.
24. Takano, S., Gately, S., Neville, M. E., Herblin, W. F., Gross, J. L., Engelhard, H., Perricone, M., Eidsvoog, K., and Brem, S. (1994) Suramin, an anticancer and angiosuppressive agent, inhibits endothelial cell binding of basic fibroblast growth factor, migration, proliferation, and induction of urokinase-type plasminogen activator. *Cancer Res. 54*, 2654–2660.
25. Morrison, R. S., Shi, E., Kan, M., Yamaguchi, F., McKeehan, W., Nawrot, M. R., and Palczewski (1994) Inositolhexakisphosphate (Ins P_6): an antagonist of fibroblast growth factor receptor binding and activity. *In Vitro Cell Dev. Biol. 30*, 783–789.
26. Vucenik, I., Passaniti, A., Vitolo, M. I., Tantivejkul, K., Eggleton, P., and Shamsuddin, A. M. (2004) Anti-angiogenic activity of inositol hexaphosphate (IP6). *Carcinogenesis 25*, 2115–2123.
27. Harland, B. F., and Oberleas, D. (1987) Phytate in foods. *World Rev. Nutr. Diet 52*, 235–259.
28. Menniti, F. S., Oliver, K. G., Pytney, J. W., Jr., and Shears, S. B. (1993) Inositol phosphates and cell signalling: new view of InsP_5 and InsP_6. *Trends Biochem. Sci. 18*, 53–65.
29. Vucenik, I., and Shamsuddin, A. M. (2003) Cancer inhibition by inositol hexaphosphate (IP6): from laboratory to clinic. *J. Nutr. 133*, 3778–3784.
30. Vucenik, I., and Shamsuddin, A. M. (2003) Protection against cancer by dietary IP6 and inositol. *Nutr. Cancer 55*, 109–125.
31. Graf, E., and Eaton, J. W. (1990) Antioxidant functions of phytic acid. *Free Radical Biol. Med. 8*, 61–69.
32. Baten, A., Ullah, A., Tomazic, V. J., and Shamsuddin, A. M. (1989) Inositol-phosphate-induced enhancement of natural killer cell activity correlates with tumor suppression. *Carcinogenesis 10*, 1595–1598.
33. Arunkumar, A. I., Kumar, T. K., Kathir, K. M., Srisailam, S., Wang, H. M., Leena, P. S., Chi, Y. H., Chen, H. C., Wu, C. H., Wu, R. T.,

Chang, G. G., Chiu, I. M., and Yu, C. (2002) Oligomerization of acidic fibroblast growth factor is not a prerequisite for its cell proliferation activity. *Protein Sci. 11*, 1050–1061.
34. Chi, Y.-H., Kumar, T. K. S., Wang, H., Ho, M.-C., Chiu, I.-M., and Yu, C. (2001) Thermodynamic characeterization of the human acidic fibroblast growth factor: evidence for cold denaturation. *Biochemistry 40*, 7746–7753.
35. Grzesiek, S., and Bax, A. (1992) Improved 3D triple-resonance NMR techniques applied to a 31 kDa protein. *J. Magn. Reson. 96*, 432–440.
36. Grzesiek, S., and Bax, A. (1993) Amino acid type determination in the sequential assignment procedure of uniformly $^{13}C/^{15}N$-enriched proteins. *J. Biomol. NMR 3*, 185–204.
37. Carlomagno, T., Maurer, M., Sattler, M., Schwendinger, M. G., Glaser, S. J., and Griesinger, C. (1996) PLUSH TACSY: Homonuclear planar TACSY with two-band selective shaped pulses applied to C-alpha, C′ transfer and C-beta, C-aromatic correlations. *J. Biomol. NMR 8*, 161–170.
38. Kay, L. E., Xu, G. Y., and Yamazaki, G. (1994) Enhanced-sensitivity triple-resonance spectroscopy with minimal H_2O saturation. *J. Magn. Reson. A 109*, 129–133.
39. Kay, L. E., Xu, G. Y., Singer, A. U., Muhandiram, D. R., and Foreman-Kay, J. D. (1993) A gradient-enhanced HCCH-TOCSY experiment for recording side-chain ^{1}H and ^{13}C correlations in H_2O samples of proteins. *J. Magn. Reson. B 101*, 333–337.
40. Schleucher, J., Schwendinger, M., Sattler, M., Schmidt, P., Schedletzky, O., Glaser, S. J., Sorensen, O. W., and Griesinger, C. (1994) A general enhancement scheme in heteronuclear multidimensional NMR employing pulsed field gradients. *J. Biomol. NMR 4*, 301–306.
41. Davis, A. L., Keeler, J., Laue, E. D., and Moskau, D. (1992) Experiments for recording pure-absorption heteronuclear correlation spectra using pulsed field gradients. *J. Magn. Reson. 98*, 207–216.
42. Breeze, A. L. (2000) Isotope-filtered NMR methods for the study of biomolecular structure and interactions. *Prog. NMR Spectrosc. 36*, 323–372.
43. Goddard, T. D., and Kneller, D. G. SPARKY 3, University of California, San Francisco.
44. Montaville, P., Coudevylle, N., Radhakrishnan, A., Leonov, A., Zweckstetter, M., and Becker, S. (2008) The PIP2 binding mode of the C2 domains of rabphilin-3A. *Protein Sci. 17*, 1025–1034.
45. Linge, J. P., O'Donoghue, S. I., and Nigles, M (2001) Assigning ambiguous NOEs with ARIA. *Methods Enzymol. 339*, 71–90.
46. Cornilescu, G., Frank, D., and Bax, A. (1999) Protein backbone angle restraints from searching a database for chemical shift and sequence homology. *J. Biomol. NMR 13*, 289–302.
47. Dominguez, C., Boelens, R., and Bonvin, A. M. J. J. (2003) HADDOCK: a protein-protein docking approach based on biochemical and/or biophysical information. *J. Am. Chem. Soc. 125*, 1731–1737.
48. De Vries, S. J., van Dijk, A. D. J., Krzeminski, M., van Dijk, M., Thureau, A., Hsu, V., Wassenaar, T., and Bonvin, A. M. J. J. (2007) HADDOCK versus HADDOCK: new features and performance of HADDOCK2.0 on the CAPRI targets. *Proteins: Struct., Funct., Bioinf. 69*, 726–733.
49. Brunger, A. T., Adams, P. D., Clore, G. M., Delano, W. L., Gros, P., Grosse-Kunstleve, R. W., Jiang, J. S., Kuszewski, J., Nilges, M., Pannu, N. S., Read, R. J., Rice, L. M., Simonson, T., and Warren, G. L. (1998) Crystallography & NMR system: a new software system for macromolecular structure determination. *Acta Crystallogr., Sect. D: Biol. Crystallogr. 54*, 905–921.
50. Kleywegt, G. J. (2007) Crystallographic refinement of ligand complexes. *Acta Crystallogr. 63*, 94–100.
51. Hubbard, S. J., and Thornton, J. M. (1993) "NACCESS", computer program, Department of Biochemistry and Molecular Biology, University College London.
52. Jorgenson, W. L., and Tirado-Rives, J. (1988) The OPLS (optimized potentials for liquid simulations) potential functions for proteins, energy minimizations for crystals of cyclic peptides and crambin. *J. Am. Chem. Soc. 110*, 1657–1666.
53. Canales-Mayordomo, A., Fayos, R., Angulo, J., Ojeda, R., Martin-Pastor, M., Nieto, P. M., Martin-Lomas, M., Lozano, R., Gimenez-Gallego, G., and Jimenez-Barbero, J. (2006) Backbone dynamics of a biologically active human FGF-1 monomer, complexed to a hexasaccharide heparin-analogue, by ^{15}N NMR relaxation methods. *J. Biomol. NMR 35*, 225–239.
54. Velazquez-Campoy, A., Vega, S., and Freire, E. (2002) Amplification of the effects of drug resistance mutations by background polymorphisms in HIV-1 protease from African subtypes. *Biochemistry 41*, 8613–8619.
55. Weber, P. C., and Salemme, R. (2003) Applications of calorimetric methods to drug discovery and the study of protein interactions. *Curr. Opin. Struct. Biol. 13*, 115–121.
56. Hibbits, K. A., Gill, D. S., and Willson, R. C. (1994) Isothermal titration calorimetric study of the association of hen egg lysozyme and the anti-lysozyme antibody HyHEL-5. *Biochemistry 33*, 3584–3590.
57. Tello, D., Goldbaum, F. A., Mariuzza, R. A., Ysern, X., Schwarz, F. P., and Poljak, R. J. (1993) Three-dimensional structure and thermodynamics of antigen binding by anti-lysozyme antibodies. *Biochem. Soc. Trans. 21*, 943–946.
58. Sturtevant, J. M. (1977) Heat capacity and entropy changes in processes involving proteins. *Proc. Natl. Acad. Sci. U.S.A. 74*, 2236–2240.
59. Ross, P. D., and Subramanian, S. (1981) Thermodynamics of protein association reactions: forces contributing to stability. *Biochemistry 20*, 3096–3102.
60. Wong, P., Hampton, B., Szylobryt, E., Gallagher, A. M., Jaye, M., and Burgess, W. H. (1995) Analysis of putative heparin-binding domains of fibroblast growth factor-1. *J. Biol. Chem. 270*, 25805–25811.
61. Spival-Kroizman, T., Lemmon, M. A., Dikic, I., Ladbury, J. E., Pinchasi, D., Huang, J., Jaye, M., Crumley, G., Schlessinger, J., and Lax, I. (1994) Heparin-induced oligomerization of FGF molecules is responsible for FGF receptor dimerization activation, and cell proliferation. *Cell 79*, 1015–1024.
62. DiGabriele, A. D., Lax, I., Chen, D. I., Svahn, C. M., Jaye, M., Schlessinger, J., and Hendrickson, W. A. (1998) Structure of a heparin-linked biologically active dimer of fibroblast growth factor. *Nature 393*, 812–817.
63. Plotnikov, A. N., Schlessinger, J., Hubbard, S. R., and Mohammadi, M. (1999) Structural basis for FGF receptor dimerization and activation. *Cell 98*, 641–650.
64. Schlessinger, J., Plotnikov, A. N., Ibrahimi, O. A., Eliseenkova, A. V., Yeh, B. K., Yayon, A., Linhardt, R. J., and Mohammadi, M. (2000) Crystal structure of a ternary FGF-FGFR-heparin complex reveals a dual role for heparin in FGFR binding and dimerization. *Mol. Cell 6*, 743–750.
65. Pineda-Lucena, A., Jimenez, M. A., Lozano, R. M., Nieto, J. L., Santoro, J., Rico, M., and Gimenez-Gallego, G. (1996) Three-dimensional structure of acidic fibroblast growth factor in solution: effects of binding to a heparin functional analog. *J. Mol. Biol. 264*, 162–178.
66. Seno, M., Sasada, R., Kurokawa, T., and Igarashi, K. (1990) Carboxy-terminal structure of basic fibroblast growth factor significantly contributes to its affinity for heparin. *Eur. J. Biochem. 189*, 239–245.
67. Imamura, T., Engleka, K., Zhan, X., Tokita, Y., Forough, R., Roeder, D., Jackson, A., Maier, J. A. M., Hla, T., and Maciag, T. (1990) Recovery of mitogenic activity of a growth factor mutant with a nuclear translocation sequence. *Science 249*, 1567–1570.